Am J Transl Res 2021;13(4):1971-1989
www.ajtr.org /ISSN:1943-8141/AJTR0129566

Original Article

Antinociceptive effects of macrophage-derived extracellular vesicles by carrying microRNA-216a

Xinxin Cai[1*], Xi Xi[2*], Xiangming Li[3], Xiaomei Zhang[3], Xiaolina Zhang[3], Zhangxiang Huang[3], Zhiwen Yan[4]

[1]Department of Anesthesiology, The First Affiliated Hospital of Kunming Medical University, Kunming 650032, Yunnan, P. R. China; [2]Department of Anesthesiology, The Second Affiliated Hospital of Kunming Medical University, Kunming 650101, Yunnan, P. R. China; [3]Department of Pain Management, The First Affiliated Hospital of Kunming Medical University, Kunming 650032, Yunnan, P. R. China; [4]Department of Anatomy, Kunming Medical University Haiyuan College, Kunming 650101, Yunnan, P. R. China. [*]Equal contributors.

Received January 5, 2021; Accepted February 7, 2021; Epub April 15, 2021; Published April 30, 2021

Abstract: Cancer-induced bone pain (CIBP) represents the pain induced by bone metastases from malignancies. The role of extracellular vesicles (Evs) has been underscored in bone metastasis. However, the function of Evs, especially these derived from M2 macrophages (M2φ-Evs) in CIBP is unclear. Therefore, this investigation aimed to probe the possible antinociceptive effect of M2φ-Evs in CIBP and the underlying mechanism of action. Using the C57bl/6 mice, a CIBP animal model was established by the administration of Walker 256 mammary gland carcinoma cells, followed by M2φ-Evs administration. It was found that CIBP mice treated with M2φ-Evs had significantly reduced nociception and serum inflammatory factors. Microarray sequencing revealed that microRNA-216a (miR-216a) was the most upregulated miRNA in Evs-treated mouse spinal cord tissues. Subsequent bioinformatics, GSEA and KEGG enrichment analyses demonstrated that HMGB1 and TLR4-NF-κB pathway were the downstream effectors of miR-216a and were both downregulated in spinal cord tissues of CIBP mice treated with M2φ-Evs. Rescue experiments displayed that after we reduced miR-216a expression in M2φ-Evs, the antinociceptive effect of M2φ-Evs on CIBP mice was inhibited, and the HMGB1 expression and the TLR4-NF-κB signaling were significantly activated. Together, M2φ-Evs relieve CIBP by carrying miR-216a, which was elicited through the HMGB1/TLR4-NF-κB axis.

Keywords: M2 macrophages, extracellular vesicles, cancer-induced bone pain, microRNA-216a, HMGB1

Introduction

Cancer pain that comes along with cancer severely distresses the quality of life of patients, and about 60%-90% of patients with advanced malignancy have been suffering from different degrees of pain, 30% of which is persistent severe pain [1]. Bone remains the third most common site of metastases (just behind the lungs and liver), and the most frequent bone metastasis stem from multiple myeloma, along with the breast, prostate, lung, thyroid, renal, as well as ovarian cancers [2]. Different from other kinds of cancer pain, cancer-induced bone pain (CIBP) is characterized by acute, inflammatory, and neuropathic pain [3]. In 1986, the WHO proposed a three-step guideline for treatment of CIBP, beginning with non-steroidal anti-inflammatory drugs (NSAIDs), to mild opiate + NSAID and finally strong opiate + NSAID [4]. Although noticeable progresses have been made in recent years, the mechanism behind CIBP has not been clearly established. Therefore, it is of paramount importance to explore new therapeutic strategies for the management and control of CIBP.

Inflammation is tightly linked to the pathobiology of CIBP through several immune cell types, and macrophages are well-known to be involved in the tumor microenvironment [5]. M2 macrophages (M2φ) are alternatively activated macrophages, and its phenotype is characterized by the secretion of anti-inflammatory cytokines and is highly linked to resolution of inflammation and tissue repair [6]. Extracellular vesicles (Evs) can be extracted from bodily fluids and tissues, and their important roles have been increasingly acknowledged in the modulation of normal physiological processes and in the

pathology of several disorders, including tumorigenesis [7]. These Evs represent a way of intercellular communication by functioning as vehicles for transfer between cells of membrane and proteins, lipids, and RNAs [8]. Moreover, Evs, comprising of microvesicles, exosomes and apoptotic vesicles, have been demonstrated to possess therapeutic potentials and might be used as biomarkers for inflammation-related diseases [9]. For instance, macrophage-derived exosomes have the potency to relieve thermal hyperalgesia related to complete Freund's adjuvant-induced inflammatory pain [10]. However, the regulatory role of M2φ-derived Evs (M2φ-Evs) in nociception in CIBP has yet to be established. In the current work, we established a mouse model with CIBP by intrathecal injection of Walker 256 mammary gland carcinoma cells, the principal challenge method for this disease [11], to study the underlying mechanism of M2φ-Evs. Meanwhile, our microRNA (miRNA) microarray analysis revealed that miR-216a was the most significantly upregulated miRNA in CIBP mice treated with M2φ-Evs. Considering all the findings, it is rational to conjecture that M2φ-Evs-carried miR-216a is associated with the nociception in CIBP. As a consequence, a string of assays was carried out later on to justify the proposition.

Materials and methods

Mouse macrophage isolation and culture

Euthanasia of mice (SPF grade, Vital River, Beijing, China, SYXK (Hu) 2017-0014) was performed by an intraperitoneal injection of overdose pentobarbital sodium at 150 mg/kg. Mice were injected intraperitoneally with 5 mL serum-free RPMI-1640 medium (#A1049101, Gibco, Carlsbad, CA, USA), and the abdomen was swabbed for 2-3 min. The peritoneum was lifted with forceps after 5 min. The peritoneal lavage fluid was then aspirated with a pipette, followed by another peritoneal lavage and a centrifugation at 204 g at 4°C for 10 min. The precipitates were suspended in RPMI-1640 medium plus 100 U/mL penicillin, 100 μg/mL streptomycin, and 10% FBS. Following adjustment of cell concentration (2×10^6 cells/mL/well) in a 24-well plate, the cells were incubated with 5% CO_2 at 37°C. After 2 to 4 h, the original medium was refreshed, and cells did not adhere to wells were removed. The monolayer cells adherent to the wells were defined as macrophages.

Induction and characterization of M2φ

Macrophages were cultured in complete medium as described above, and M2-like macrophages was harvested by a 24-h incubation with mouse IL-4 (Sigma-Aldrich, St Louis, MO, USA) at 20 ng/mL [12]. Macrophages were suspended in 5 μL PBS, dropped onto slides, dried, added to Wright's staining solution, stained with buffer solution (1:2) for 10 min, air-dried, and viewed under a microscope. For flow cytometric analysis, samples to be tested (1×10^6) were suspended, and ice-bathed with 2 μL fluorescent antibody Alexa Fluor® 647 conjugated CD68 (1:100, ab31630, Abcam, Cambridge, UK) and Alexa Fluor® 488 conjugated CD163 (1:60, ab182422, Abcam) or control IgG1 (1:500, ab170190, Abcam) for 0.5 h, rinsed with fluorescence-activated cell sorting buffer, followed by fixation using 10% formalin. The positive rate of the antigen was assessed with the help of flow cytometry ($CD68^+$ purity 98.97% and $CD163^+$ purity 99.04%).

Preparation of conditioned medium (CM) and characterization of M2φ-Evs

M2φ cultured in Evs-free RPMI-1640 medium containing the mixture of 100 U/mL penicillin, 100 μg/mL streptomycin, and 10% FBS were subjected to a 200,000 g centrifugation for 18 h to remove Evs. The supernatant was harvested after a 10-min centrifugation at 700 g and used as CM (M2-CM).

Evs were isolated from M2-CM with ultra-centrifugations. In brief, Evs were pre-fixed with 2.5% glutaraldehyde (pH = 7.4) in PBS for 120 min and then fixed with 1% tetraoxide in PBS for another 120 min. Evs were loaded onto glow-discharged copper grids for 1 min and stained with 2% phosphotungstic acid aqueous solution. The copper grid was stained with 2% uranyl acetate for 40 s. After being air-dried at ambient temperature, the samples were observed under a TEM at 80 keV. Evs were diluted to 1 mL in tris(pyrazolyl)methane. The size and concentration of Evs were evaluated using the ZetaView PMX 110 (Particle Metrix GmbH, Microtrac, Melbosch, Germany), along with Nanosight Tracking Analysis. Western blot was then conducted to determine the levels of CD63

(1:1000, ab59479), CD81 (1:1000, ab79559) and TSG101 (1:1000, ab30871) (all from Abcam).

Establishment of a CIBP mouse model

Animal assays were performed as per the NIH Guide for the Care and Use of Laboratory Animals and were ratified by the Ethics Committee of the First Affiliated Hospital of Kunming Medical University. Walker 256 cells were cultured in Walker 256 cell culture medium (Sigma) plus 10% horse serum (Gibco, Carlsbad, CA, USA) and maintained at 37°C with 5% CO_2 (Thermo Fisher Scientific Inc., Waltham, MA, USA). The CIBP mouse model was established as previously described [13]. Ninety-six mice (20 ± 2 g, 4-6 weeks, Vital River) were anesthetized intraperitoneally with pentobarbital sodium at 50 mg/kg. Right knee arthroplasty was performed after general anesthesia. Next, 20 μL α-minimum essential medium (α-MEM, #12000063, Thermo Fisher Scientific) containing 2 × 10^5 Walker 256 cells was injected into the medullary cavity of the right femur, while 20 μL α-MEM was injected into the sham-operated mice. After sealing the drilled holes with bone wax, the wounds were sutured with 4-0 silk sutures (Ethicon, INC., Somerville, NJ, USA). The animals recovered from anesthesia on heated blankets.

To clarify the nociception of mice caused by M2φ-Evs, we injected PBS or gradient concentrations of Evs intrathecally into the spinal cord tissue of mice at the L4 to L6 level. Subsequently, the adenoviral overexpression vector for HMGB1 (AAV9-HMGB1) as well as the corresponding empty vector AAV9-NC were injected intrathecally into M2φ-Evs-treated mice.

Behavioral nociceptive tests

Mice were tested for mechanical allodynia (evoked nociception) and spontaneous nociception before surgery (day 0) and 4, 7, 10, 14, 21, and 28 days following surgery, and 0, 1, 3, and 6 h after M2φ-Evs treatment. Behavioral nociceptive tests were conducted by two experimenters who had no knowledge of the grouping information.

Mechanical allodynia was determined using von Frey monofilaments (Stoelting, Wood Dale, IL, USA). The paw withdrawal mechanical threshold (PWMT) was evaluated as described previously [14]. Briefly, the mice were placed in a Plexiglas sleeve (18 × 6 × 6 cm) equipped with a metal mesh at the bottom, 15 min prior to first stimulation. Starting at 0.41 g, stimulation applied in an ascending intensity (0.41 g, 0.70 g and 1.20 g) until the first paw withdrawal response. An ascending intensity of 2.00 g, 3.63 g, 5.50 g, 8.50 g, and 15.10 g was applied to the plantar surface of the hind paws of mice to observe the presence of a withdrawal response. Positive responses were recorded once mice developed a rapid foot withdrawal response during stimulation or when the von Frey filaments were removed. If a positive response occurred, von Frey stimulation was applied with the adjacent lower intensity and continued until the first positive and negative (or negative and positive) responses occurred, followed by five successive stimulations in ascending or descending orders, depending on the response. It took a few seconds between different stimulations to eradicate the effects of the previous response.

The mice were placed in a clear Plexiglas compartment with a wire mesh bottom and acclimatized for 0.5 h, after which the number of spontaneous flinches (NSF) of the right hind paw was measured over 2 min. Each mouse was tested for five times. All mice were successfully modeled based on the results of behavioral nociceptive tests.

After completion of behavioral nociceptive tests, mice were euthanized as described above. Subsequently, the spinal cord tissues of mice at the L4 to L6 level were extracted. In brief, the skin of the back of the mice was cut open, and the spine was isolated. The spine was cut inferiorly at the line joining the iliac spine on both sides, and superiorly at the rib arch below the lumbar spine. The removed spinal tissues were quickly cooled on ice, and gently flushed out by drawing ice saline with a 20 mL syringe. The intumescentia lumbalis of the spinal cord tissue was gently cut and rinsed with saline. The spinal cord tissues were then placed in an Eppendorf (EP) tube and stored at -80°C.

Histological staining

The frozen longitudinal sections of the spinal cord were rinsed 3 times (5 min each) with PBS and blocked in PBS containing 5% normal goat

Table 1. Primer sequences of RT-qPCR

Targets	Forward (5'-3')	Reverse (5'-3')
miR-216a	TCTCAGCTGGCAACTGTG	GAACATGTCTGCGTATCTC
miR-392	TGGTCCGTGGCGCGTTC	GAACATGTCTGCGTATCTC
miR-6857	TTGGGGATTGGGTCAGGCC	GAACATGTCTGCGTATCTC
miR-337	AACGGCGTCATGCAGGAG	GAACATGTCTGCGTATCTC
miR-24	GCCTACTGAGCTGAAACAG	GAACATGTCTGCGTATCTC
U6	CTCGCTTCGGCAGCACAT	TTTGCGTGTCATCCTTGCG
CCL22	GTGGAAGACAGTATCTGCTGCC	AGGCTTGCGGCAGGATTTTGAG
PPARγ	GTACTGTCGGTTTCAGAAGTGCC	ATCTCCGCCAACAGCTTCTCCT
HMGB1	CCAAGAAGTGCTCAGAGAGGTG	GTCCTTGAACTTCTTTTTGGTCTC
GAPDH	CATCACTGCCACCCAGAAGACTG	ATGCCAGTGAGCTTCCCGTTCAG

Note: RT-qPCR, reverse transcription quantitative polymerase chain reaction; miR, microRNA; CCL22, C-C motif chemokine ligand 22; PPARγ, peroxisome proliferator-activated receptor gamma; HMGB1, high mobility group box 1; GAPDH, glyceraldehyde-3-phosphate dehydrogenase.

serum and 0.4% Triton X-100 for 60 min at ambient temperature. Sections were probed overnight with the primary antibodies to polyclonal rabbit antibody to toll-like receptor 4 (TLR4, 1:300, #14358, Cell Signaling Technologies, Beverly, MA, USA), phos-IKKB (1:300, #9958, Cell Signaling Technologies), or phos-p65 (1:100, ab76302, Abcam) at 4°C. Afterwards, the sections were re-probed with the secondary antibodies to horseradish peroxidase (HRP, 1:5000, #G-21234)- or Alexa fluorophore-coupled secondary antibody (1:3000, #A32727, Invitrogen Inc., Carlsbad, CA, USA) for 60 min at ambient temperature. A Zeiss Imager M2 upright microscope was applied for observation, and immunostaining was quantified using MetaMorph software.

Hematoxylin-eosin (HE) staining

After the sections were hydrated, the slides were immersed in water and in hematoxylin (GHS332-1 L; Sigma-Aldrich) for 3 min, followed by eosin solution staining (diluted at 1:3 in 80% ethanol) for 45 s. The slides were dehydrated, cleared in xylene, covered with Permount (SP15-100; Fisher Scientific Company, Toronto, Canada, Canada) and dried overnight.

MiRNA microarray

MiRNA microarrays of spinal cord tissues from Ev- or PBS-treated mice (n = 3) were commissioned to OE Biotech Company (Shanghai, China). The fragment mixture was hybridized with Agilent Mouse microRNA array 21.0 (8 × * 60 K, Design ID: 070155). The miRNA 4.0 platform from Affymetrix (Santa Clara, CA, USA) was applied for microarray analysis. Samples were labeled, hybridized and washed as per the manufacturer's protocol (Agilent Technologies, Santa Clara, CA, USA). Fold change cutoffs ≥ 2 for up- and down-regulated genes were used as the criteria.

RT-qPCR

Briefly, L4-L6 spinal cord tissues were placed in 1.5 mL EP tube and lysed with 10 × Trizol. The tissues were then mixed with 1/5 chloroform for 15-30 s, allowed to stand at ambient temperature for 5 min, and centrifuged at 12,000 × g at 4°C for 15 min. The upper aqueous phase was then placed at ambient temperature for 10 min with an equal volume of isopropanol and centrifuged for 10 min at 4°C at 12,000 × g. After centrifugation, the samples were dried, and approximately 20 μL RNase Free in water was used for quantification. The reliability of the obtained RNA was subsequently verified using formaldehyde denaturation electrophoresis assay. Subsequently, RT-qPCR experiments were performed using the PrimeScript™ RT kit (#RR037A, TAKARA, Otsu, Shiga, Japan) in strict accordance with the instructions. The mRNA expression was quantified by standard RT-qPCR methods using SYBR Premix Ex Taq (#RR820A, TAKARA). The relative expression was calculated as $2^{-\Delta Ct}$(specific gene)/$2^{-\Delta Ctmean}$, using the gene encoding glyceraldehyde phosphate dehydrogenase (GAPDH) as the endogenous housekeeping control gene. Primer sequences in **Table 1** were synthesized by Sangon (Shanghai, China).

Western blot

Protein was extracted from L4-L6 segments of spinal cord tissues. A total of 40 mg protein per sample was separated using 8-10% SDS-PAGE and transferred to membranes. Western blot analysis of polyvinylidene fluoride membranes (Merck Millipore, Darmstadt, Germany) was performed by an electroblotter (Bio-Rad, Hercules, CA, USA). The membranes were sealed with 5% skim milk in TBST for 60 min and incubated

with primary antibodies to high mobility group box-1 (HMGB-1, 1:1,000, ab18256, Abcam), TLR4 (1:1000, #14358, Cell Signaling Technologies), phos-IKKB (1:2000, #9958, Cell Signaling Technologies), phos-p65 (1:1,000, ab76302, Abcam), and GADPH (1:1000, Solarbio, Beijing, China) overnight at 4°C. The HRP-conjugated secondary antibody (Cell Signaling Technology) was used for re-probing for 60 min at ambient temperature. The sites of antigen-antibody complexes can be viewed using Immobilon Western chemiluminescent HRP substrates (#WBKLS0050, Millipore). Bands were analyzed by Quantity One software (Bio-Rad).

ELISA

To determine the concentration of inflammatory cytokines, serum levels of IL-1β, tumor necrosis factor-α (TNF-α), and IL-6 were measured in mice. The analysis was performed using the mouse IL-1β (PI301), TNF-α (PT512), and IL-6 (PI326) ELISA kits (Beyotime Biotechnology, Shanghai, China) following the manufacturer's protocols.

Dual-luciferase analysis

Sequences corresponding to HMGB1 mRNA 3'untranslated region (3'UTR) and containing wild-type (wt) or mutant (mt) of miR-216a binding sequences were produced by GeneScript (Nanjing, Jiangsu, China). These sequences were cloned into the FseI and XbaI restriction sites of the pGL3 luciferase control reporter vectors (Promega, Madison, WI, USA) to create HMGB1 3'-UTR reporter gene constructs (pGL3-WT-HMGB1 and pGL3-MUT-HMGB1). 293T cells were plated into 24-well plates and cultured for 1 d prior to transfection. 293T cells treated with miR-216a mimic or mimic control were plated into 96-well plates and co-transfected with pGL3-WT-HMGB1 or pGL3-MUT-HMGB1 3'-UTR (100 ng). The luciferase activity was assessed using the Dual-Luciferase Reporter Assay System (Promega, Madison, WI, USA).

Data statistics

Data were analyzed in GraphPad Prism 8.0 (Graph Pad Inc, CA, USA) and SPSS 25.0 (IBM Corp. Armonk, N.Y., USA). All data are exhibited as mean ± SD, and the level of significance was set to $P < 0.05$. The comparison of measurement data was conducted using unpaired *t*-test. The comparison of differences among each group was conducted using one-way or two-way ANOVA, followed by Tukey's post-hoc analysis.

Results

Characterization of M2φ and M2φ-Evs

After cell isolation and the initial culture, the macrophages were stained by Wright's staining. We observed that the macrophages were irregularly shaped, with dark blue nuclei, and exhibited typical macrophage morphological features (**Figure 1A**). Moreover, flow cytometric analysis exhibited that the extracted cells were double positive for CD68 and CD163, the macrophage-specific molecular markers (**Figure 1B**). IL-4 was used to induce M2-like macrophages. M2-like macrophages were markedly enlarged and predominantly appeared as round cells under the microscope (**Figure 1C**). The expression patterns of CCL22 and PPARγ were then examined in M2-like macrophages using RT-qPCR. The expression of CCL22 and PPARγ at mRNA level was increased (**Figure 1D**, **1E**), indicating successful induction of M2φ. Evs were isolated from M2-CM. The morphology was viewed under TEM (**Figure 1F**). The average size distribution of the Evs was approximately 100 nm (**Figure 1G**). These Evs were positive for the expression of CD63, CD81, and TSG101 (**Figure 1H**).

CIBP mouse model is successfully developed

Walker 256 cells were intrathecally injected to create a murine CIBP model. Evoked nociception and spontaneous nociception were measured by determining the PWMT (**Figure 2A**) and NSF (**Figure 2B**) on postoperative days 0, 4, 7, 10, 14, 21, and 28. We found no notable difference in the PWMT and NSF between sham-operated and tumor-bearing mice on days 0 to 4. From day 7 in the sham-operated mice, the surgery has resulted in mechanical hypersensitivity due to recovery of nociception. In the tumor-bearing mice, the PWMT decreased from day 10, and the NSF continued to increase until day 28. Both PWMT and NSF showed statistically significant differences in tumor-bearing mice versus the sham-operated mice on postoperative days 10, 14, 21, and 28. Hematoxylin and eosin staining of femoral sections

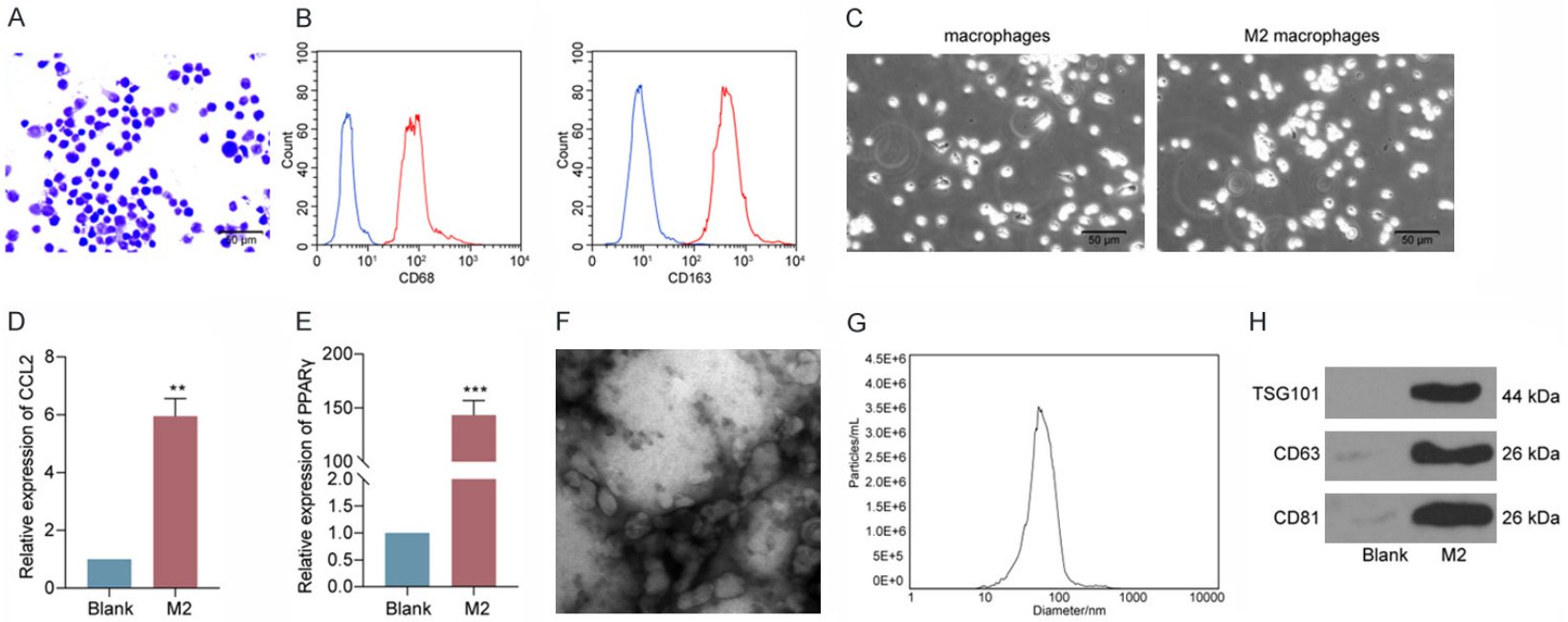

Figure 1. Characterization of M2φ and M2φ-Evs. A. Morphology of macrophage detected by Wright's staining; B. The expression of CD68 and CD163 assessed by flow cytometry; C. The macrophage and M2-like macrophage morphology observed by an optical microscope; D. CCL22 expression determined by RT-qPCR; E. PPARγ expression evaluated by RT-qPCR; F. Observation of the size distribution of M2φ-Evs by TEM; G. M2φ-Evs particle size by Nanosight Tracking Analysis; H. Expression of CD63, CD81 and TSG101 measured by western blot analysis.

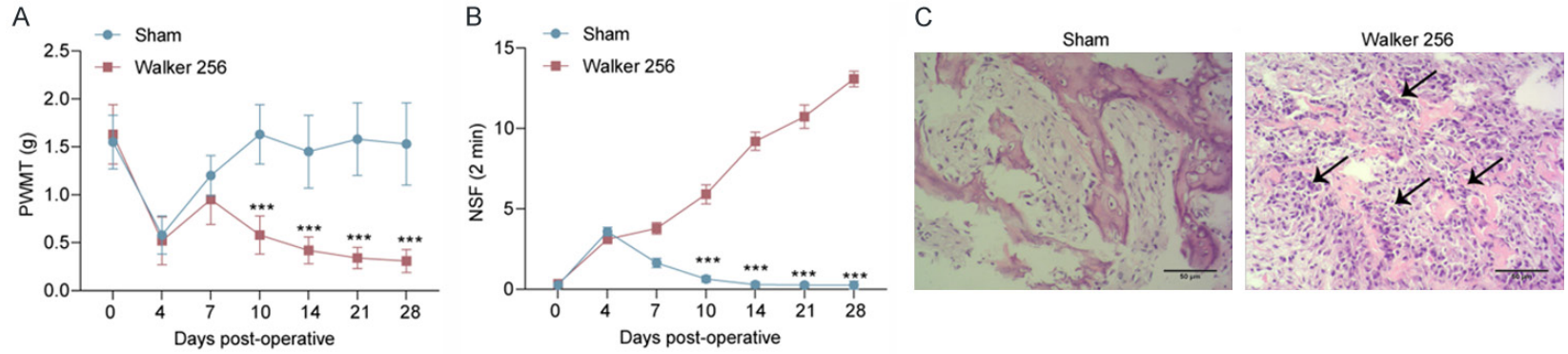

Figure 2. CIBP mice are successfully induced. A. Mean (± SD) PWMT (in g) in response to five von Frey hair stimulations; B. NSF within 2 min; C. HE staining of the femoral medullary cavity in the sham-operative and tumor-bearing mice on postoperative day 14. n = 8. ***$P < 0.001$ as determined by one-way (*vs* day 0) or two-way ANOVA (*vs* sham-operated mice), followed by Tukey's post-hoc analysis.

showed tumor cell infiltration, discontinuous trabeculae, and destruction of bone cortex in the marrow cavity of CIBP mice on postoperative day 14 (**Figure 2C**).

Intrathecal injection of M2φ-Evs reduces nociception in mice with CIBP

In order to investigate the mitigating effect of M2φ-Evs on the nociception in CIBP mice, we injected gradient concentrations of M2φ-Evs into CIBP mice by intrathecal injection (**Figure 3A**). A significant increase in the PWMT (**Figure 3B**) and a significant decline in NSF (**Figure 3C**) were observed in mice following treatment with M2φ-Evs. This indicates that M2φ-Evs treatment can significantly reduce the nociception in the CIBP mouse model.

Subsequently, we further examined the TNF-α, IL-1β, and IL-6 levels in mouse serum. It was observed that levels of inflammatory factors were much higher in mice inoculated with Walker 256 cells, but further M2φ-Evs treatment significantly lowered the levels of these inflammatory factors in mouse serum (**Figure 3D**). The activation of glial cells in spinal cord tissues was significantly correlated with the development of inflammatory response and nociception, so we further used RT-qPCR and immunofluorescence to detect the expression of the glial activation marker GFAP in mouse spinal cord tissues. The expression of GFAP was remarkably increased in the spinal cord tissues of Walker 256-injected mice, while M2φ-Evs treatment significantly reduced glial cell activation (**Figure 3E**, **3F**). Moreover, we found that the alleviating effect on nociception in CIBP mice increased significantly with the increase of Ev concentration.

M2φ-Evs mitigates the nociception in CIBP mice by delivering miR-216a

Subsequently, we used a miRNA microarray to analyze the differential expressed miRNAs in the spinal cord tissues of PBS-treated and M2φ-Evs-treated mice, and we screened a total of 196 differentially expressed miRNAs. Thirty-four of these miRNAs were significantly reduced, 162 were significantly upregulated (**Figure 4A**), and the heatmap shows the top 15 differentially expressed miRNAs (**Figure 4B**). Subsequently, we used RT-qPCR to measure the expression of the top six miRNAs in the spinal cord tissues of M2φ-Evs-treated mice, and we found the most significant difference in the miR-216a expression (**Figure 4C**). Furthermore, we analyzed the distribution of miR-216a via the RNAlocate website (http://www.rna-society.org/rnalocate/index.html) and miR-216a is predominantly found in exosomes (**Figure 4D**).

Reduction of miR-216a attenuates the antinociceptive effect of M2φ-Evs on CIBP mice

We subsequently transfected miR-216a inhibitor into M2 macrophages before extracting Evs for detection of the antinociceptive effects of miR-216a on CIBP mice. We first detected miR-216a expression in M2φ as well as in M2φ-Evs using RT-qPCR, which confirmed the reduction of miR-216a (**Figure 5A**) carried by M2φ-Evs. We then used a dose of 40 μg/mL M2φ-Evs for treatment of CIBP mice. First, detection of PWMT and NSF revealed a significant decrease in PWMT and a significant augment in NSF in CIBP mice following reduction of M2φ-Evs carrying miR-216a (**Figure 5B**, **5C**). Moreover, we used ELISA to measure the levels of inflammatory factors in mouse serum, and we noted that the serum levels of TNF-α, IL-1β, and IL-6 had a significant enhancement after reducing miR-216a in M2φ-Evs (**Figure 5D**). Again, we tested the activation level of glial cells in spinal cord tissues. GFAP expression had a significant elevation after reducing miR-216a in M2φ-Evs (**Figure 5E**, **5F**).

miR-216a targets HMGB1 and negatively regulates its expression

To further define the downstream regulatory mechanism of miR-216a, we used StarBase (http://starbase.sysu.edu.cn/), miRDB (http://mirdb.org/), and TargetScan (http://www.targetscan.org/vert_72/) to predict and screen target genes for miR-216a, and we screened 155 genes (**Figure 6A**). Subsequently, we used the DAVID 6.7 bioinformatics website (https://

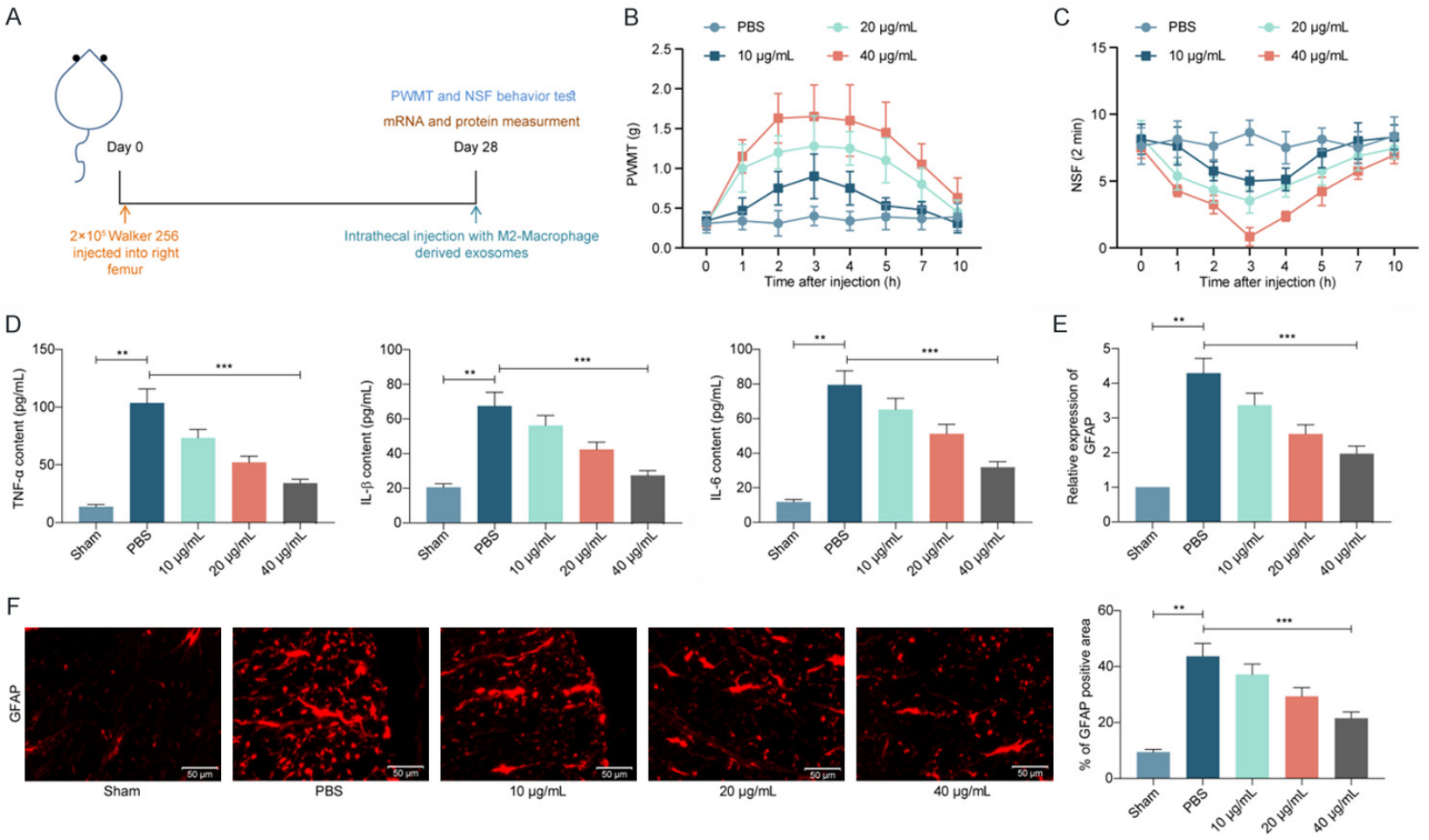

Figure 3. Intrathecal injection of M2φ-Evs reduces the nociception in mice with CIBP. M2φ-Evs at different concentrations (10 μg/mL, 20 μg/mL and 40 μg/mL) were injected into CIBP mice with PBS as control. (A) Timeline of *in vivo* experiments; (B) Mean (± SD) PWMT (in g) in response to five von Frey hair stimulations; (C) NSF in a time span of 2 min; (D) ELISA detection of inflammatory factors TNF-α, IL-1β, IL-6 in mouse serum; (E, F) Expression of the glial activation marker GFAP in mouse spinal cord tissues was detected by RT-qPCR (E) and immunofluorescence (F). n = 8. **P < 0.01, ***P < 0.001 as determined by one-way (D-F) or two-way ANOVA (B and C), followed by Tukey's post-hoc analysis.

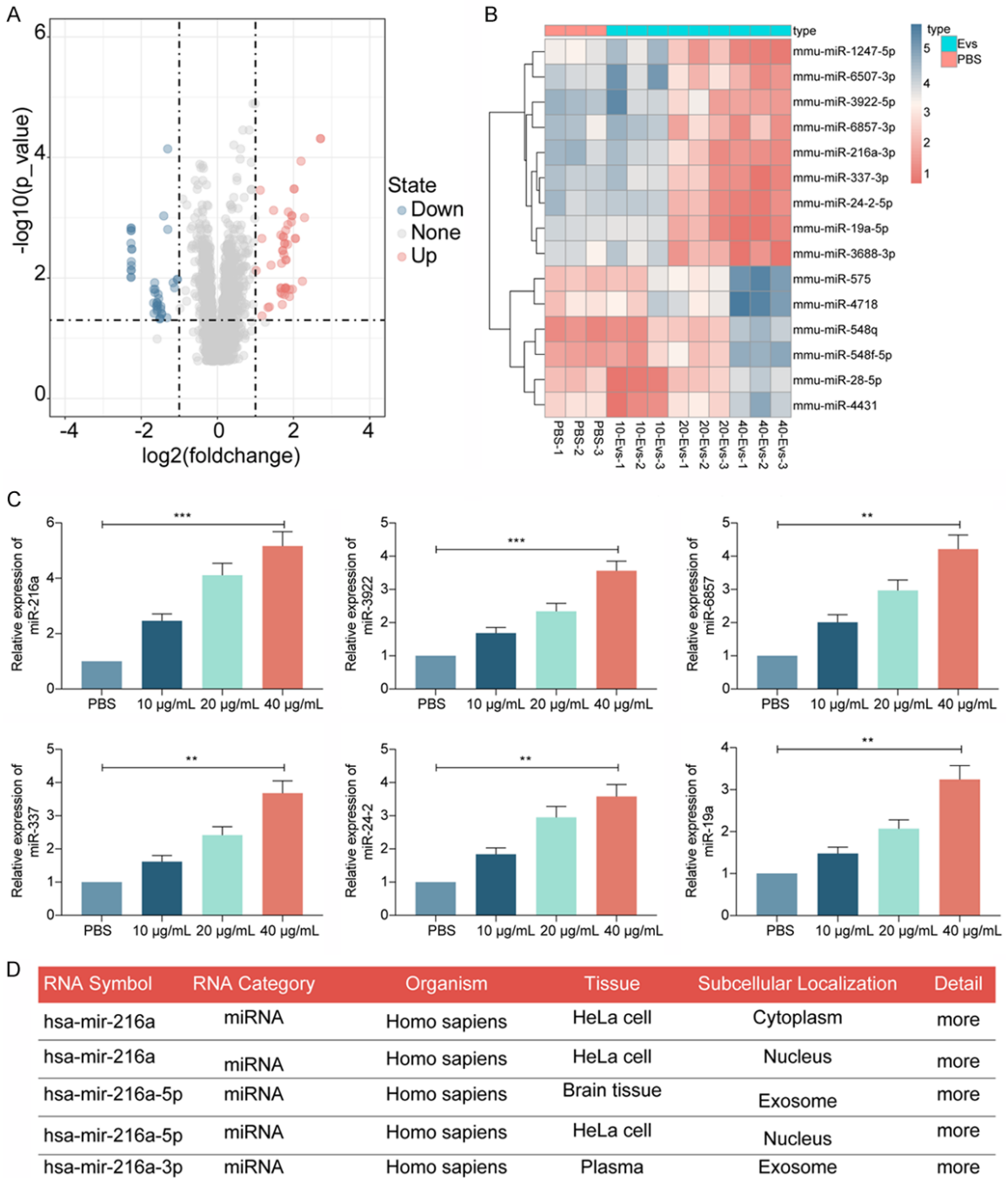

D

RNA Symbol	RNA Category	Organism	Tissue	Subcellular Localization	Detail
hsa-mir-216a	miRNA	Homo sapiens	HeLa cell	Cytoplasm	more
hsa-mir-216a	miRNA	Homo sapiens	HeLa cell	Nucleus	more
hsa-mir-216a-5p	miRNA	Homo sapiens	Brain tissue	Exosome	more
hsa-mir-216a-5p	miRNA	Homo sapiens	HeLa cell	Nucleus	more
hsa-mir-216a-3p	miRNA	Homo sapiens	Plasma	Exosome	more

Figure 4. M2φ-Evs mitigates the nociception in CIBP mice by delivering miR-216a. (A) Microarray analysis of miRNA expression differences in spinal cord tissues from PBS-treated and M2φ-Evs-treated mice; (B) The heatmap showing the top 15 differentially expressed miRNAs; (C) The expression of the top six miRNAs in the spinal cord tissues of M2φ-Evs-treated mice examined by RT-qPCR; (D) Analysis of miR-216a distribution in cells via the RNAlocate website. $^{**}P < 0.01$, $^{***}P < 0.001$ as determined by one-way ANOVA (C), followed by Tukey's post-hoc analysis.

david.ncifcrf.gov/) for KEGG functional enrichment of the selected genes, and we found that TLR4 and the NF-κB signaling pathway were significantly enriched (**Figure 6B**, **6C**). Furthermore, it has been shown in a previous study that miR-34a alleviates spinal injury by targeting HMGB1 to downregulate the activity of the TLR4 signaling pathway [15]. In our CIBP mouse model, HMGB1 expression was significantly increased, but further treatment with M2φ-Evs significantly decreased HMGB1 expression. Reducing miR-216a in M2φ-Evs, accordingly, sig-

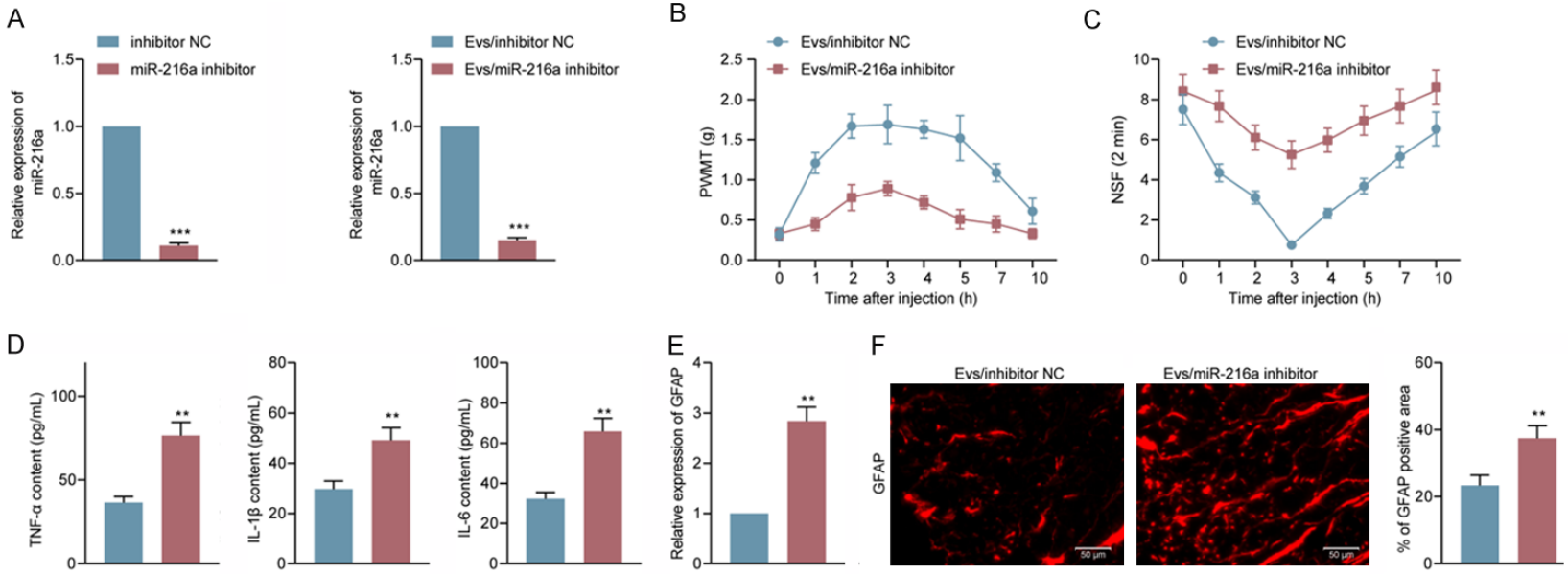

Figure 5. Reduction of miR-216a attenuates the antinociceptive effect of M2φ-Evs on CIBP mice. CIBP mice were treated with Evs extracted from M2φ transfected with miR-216a inhibitor or inhibitor NC, (A) miR-216a expression in M2φ and in Evs examined by RT-qPCR; (B) Mean (± SD) PWMT (in g) in response to five von Frey hair stimulations; (C) NSF in a time span of 2 min; (D) ELISA detection of inflammatory factors TNF-α, IL-1β, IL-6 in mouse serum; (E, F) Expression of the glial activation marker GFAP in mouse spinal cord tissues was detected by RT-qPCR (E) and immunofluorescence (F). n = 8. $^{**}P < 0.01$, $^{***}P < 0.001$ as determined by unpaired *t* test (A, D-F) or two-way ANOVA (B and C), followed by Tukey's post-hoc analysis.

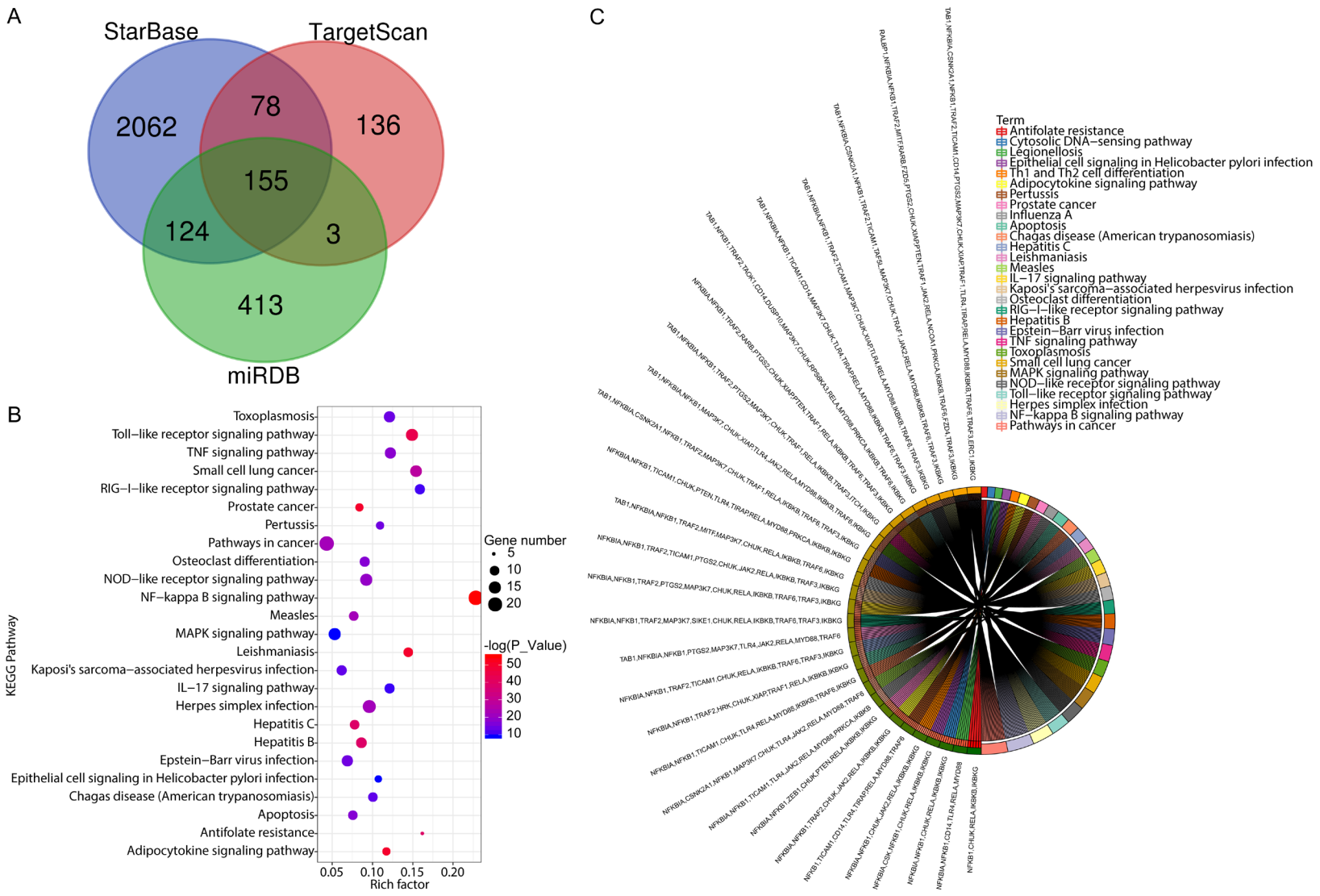
A
StarBase
TargetScan
miRDB
2062
78
136
155
124
3
413
B
KEGG Pathway
Toxoplasmosis
Toll−like receptor signaling pathway
TNF signaling pathway
Small cell lung cancer
RIG−I−like receptor signaling pathway
Prostate cancer
Pertussis
Pathways in cancer
Osteoclast differentiation
NOD−like receptor signaling pathway
NF−kappa B signaling pathway
Measles
MAPK signaling pathway
Leishmaniasis
Kaposi's sarcoma−associated herpesvirus infection
IL−17 signaling pathway
Herpes simplex infection
Hepatitis C
Hepatitis B
Epstein−Barr virus infection
Epithelial cell signaling in Helicobacter pylori infection
Chagas disease (American trypanosomiasis)
Apoptosis
Antifolate resistance
Adipocytokine signaling pathway
0.05
0.10
0.15
0.20
Rich factor
Gene number
5
10
15
20
-log(P_Value)
50
40
30
20
10
C
Term
Antifolate resistance
Cytosolic DNA−sensing pathway
Legionellosis
Epithelial cell signaling in Helicobacter pylori infection
Th1 and Th2 cell differentiation
Adipocytokine signaling pathway
Pertussis
Prostate cancer
Influenza A
Apoptosis
Chagas disease (American trypanosomiasis)
Hepatitis C
Leishmaniasis
Measles
IL−17 signaling pathway
Kaposi's sarcoma−associated herpesvirus infection
Osteoclast differentiation
RIG−I−like receptor signaling pathway
Hepatitis B
Epstein−Barr virus infection
TNF signaling pathway
Toxoplasmosis
Small cell lung cancer
MAPK signaling pathway
NOD−like receptor signaling pathway
Toll−like receptor signaling pathway
Herpes simplex infection
NF−kappa B signaling pathway
Pathways in cancer

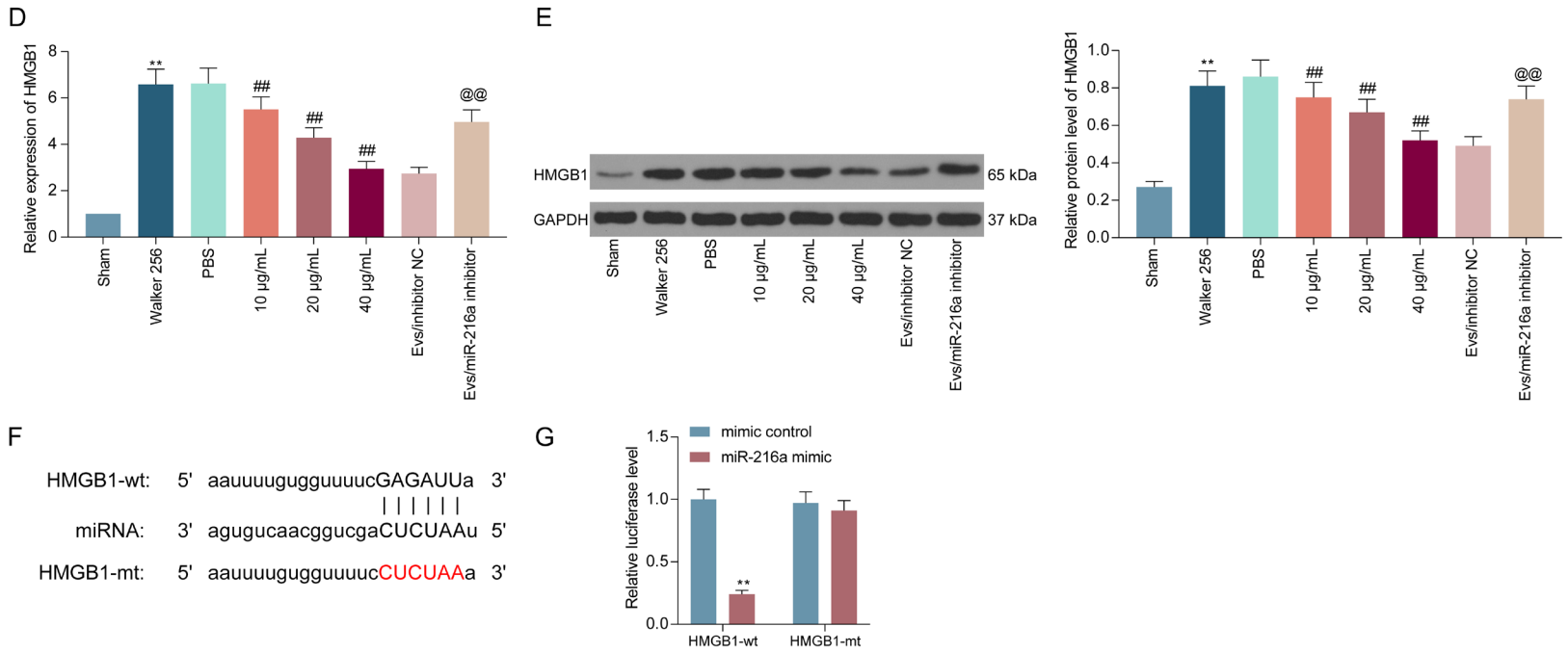

Figure 6. miR-216a targets HMGB1. (A) Prediction and screening of target mRNAs for miR-216a using StarBase, miRDB, and TargetScan; (B, C) The bubble map (B) and pie chart (C) for the KEGG enrichment analysis; (D, E) Expression of HMGB1 in mouse spinal cord tissues detected by RT-qPCR (D) and Western blot (E); (F) The predicted binding sites of miR-216a in the 3'UTR of HMGB1; (G) The results of luciferase reporter assays performed after co-transfection of 293T cells with a pGL3 construct containing the wt or mt HMGB1 3'-UTR region and miR-216a mimic. n = 8. $^{**}P < 0.01$, $^{\#\#}P < 0.01$, $^{@@}P < 0.01$ as determined by one-way ANOVA (D and E) or two-way ANOVA (G), followed by Tukey's post-hoc analysis.

nificantly promoted HMGB1 expression (**Figure 6D**, **6E**). To further determine the binding relation between miR-216a and HMGB1, we designed a dual-luciferase assay and observed that luciferase activity was significantly diminished in 293T cells co-transfected with miR-216a mimic and HMGB1-wt, but not in cells treated with mimic control or HMGB1-mt (**Figure 6F**, **6G**).

HMGB1 promotes nociception in CIBP mice through activating the TLR4-NF-κB signaling

In the **Figure 6**, we substantiated that M2φ-Evs can inhibit HMGB1 expression by delivering miR-216a. Moreover, HMGB1 was found to activate the TLR4 signaling pathway in a previous report. Therefore, western blot was conducted to assess the TLR4 expression and the extents of IKKB and NF-κB p65 phosphorylation in mouse spinal cord tissues. The TLR4 expression and the extent of IKKB and NF-κB p65 phosphorylation were remarkably boosted after Walker 256 cell inoculation, but the activation level of the TLR4-NF-κB signaling was remarkably inhibited after M2φ-Evs treatment. However, after further reduction of miR-216a in M2φ-Evs, the expression of TLR4 and the phosphorylation levels of IKKB and NF-κB p65 in tissues had a significant restoration (**Figure 7A**). Similarly, the staining intensities of TLR4, phos-IKKB, and phos-NF-κB p65 in spinal cord tissues were measured by immunohistochemistry, with experimental results consistent with western blot (**Figure 7B-D**).

AAV9-HMGB1 attenuates the blocking effect of M2φ-Evs on TLR4-NF-κB signaling

To probe the role of HMGB1 on the nociception in CIBP mice, we administrated HMGB1 adenovirus overexpression vector (AAV9-HMGB1) into M2φ-Evs-treated mice by intrathecal injection. We examined the TLR4 expression and the IKKB and NF-κB p65 phosphorylation levels in spinal cord tissues using western blot and found that after overexpressing HMGB1, expression of TLR4 as well as extent of IKKB and NF-κB p65 phosphorylation were notably increased (**Figure 8A**). Thereafter, we tested the PWML and NSF of each group of mice and observed that after M2φ-Evs treatment and further overexpression of HMGB1, CIBP mice had a significant decline in PWMT and a significant augment in NSF (**Figure 8B**, **8C**). Also, the serum levels of inflammatory factors were drastically elevated in the mice (**Figure 8D**). And, we further tested the activation levels of glial cells in spinal cord tissues. GFAP expression levels were significantly promoted after overexpression of HMGB1 (**Figure 8E**, **8F**).

LPS attenuates the antinociceptive effect of M2φ-Evs on CIBP mice

To further determine that M2φ-Evs alleviate nociception in CIBP mice by blocking the TLR4-NF-κB signaling, we injected LPS intrathecally into M2φ-Evs-treated mice. TLR4 expression as well as phosphorylated IKKB and NF-κB p65 were significantly restored after LPS treatment (**Figure 9A**). Subsequently, we tested the PWMT and NSF of each group of mice and found that after M2φ-Evs treatment and further use of LPS, CIBP mice had a significant decline in PWMT and a significant elevation in NSF (**Figure 9B**, **9C**). Also, the serum levels of inflammatory factors were considerably induced in the mice (**Figure 9D**). We further tested the activation level of glial cells in spinal cord tissues and observed that the expression of GFAP was significantly elevated after TLR4-NF-κB signaling activation (**Figure 9E**, **9F**). In conclusion, M2φ-Evs target and negatively regulate HMGB1 expression by carrying miR-216a and therefore downregulate the TLR4-NF-κB signaling pathway, resulting in an antinociceptive effect in a mouse model of CIBP (**Figure 10**).

Discussion

Bone metastases involve a multifaceted process involving interplay between disseminated cancer cells and the bone microenvironment, and the discovery of Evs in the body fluids opened new frontiers regarding the possibility of reducing metastases as well as identifying novel therapeutic approaches [16]. This study set to elucidate the possible molecular mechanisms of miR-216a transferred by M2φ-Evs in CIBP by inducing a mouse model. We proposed that miR-216a transferred by M2φ-Evs exerted antinociceptive effects on CIBP mice by suppressing HMGB1 expression and impairing the TLR4-NF-κB signaling pathway. These findings might be beneficial for the treatment of CIBP in later clinical setting.

Our initial observation was that M2φ-Evs remarkably reduced the levels of pro-inflammato-

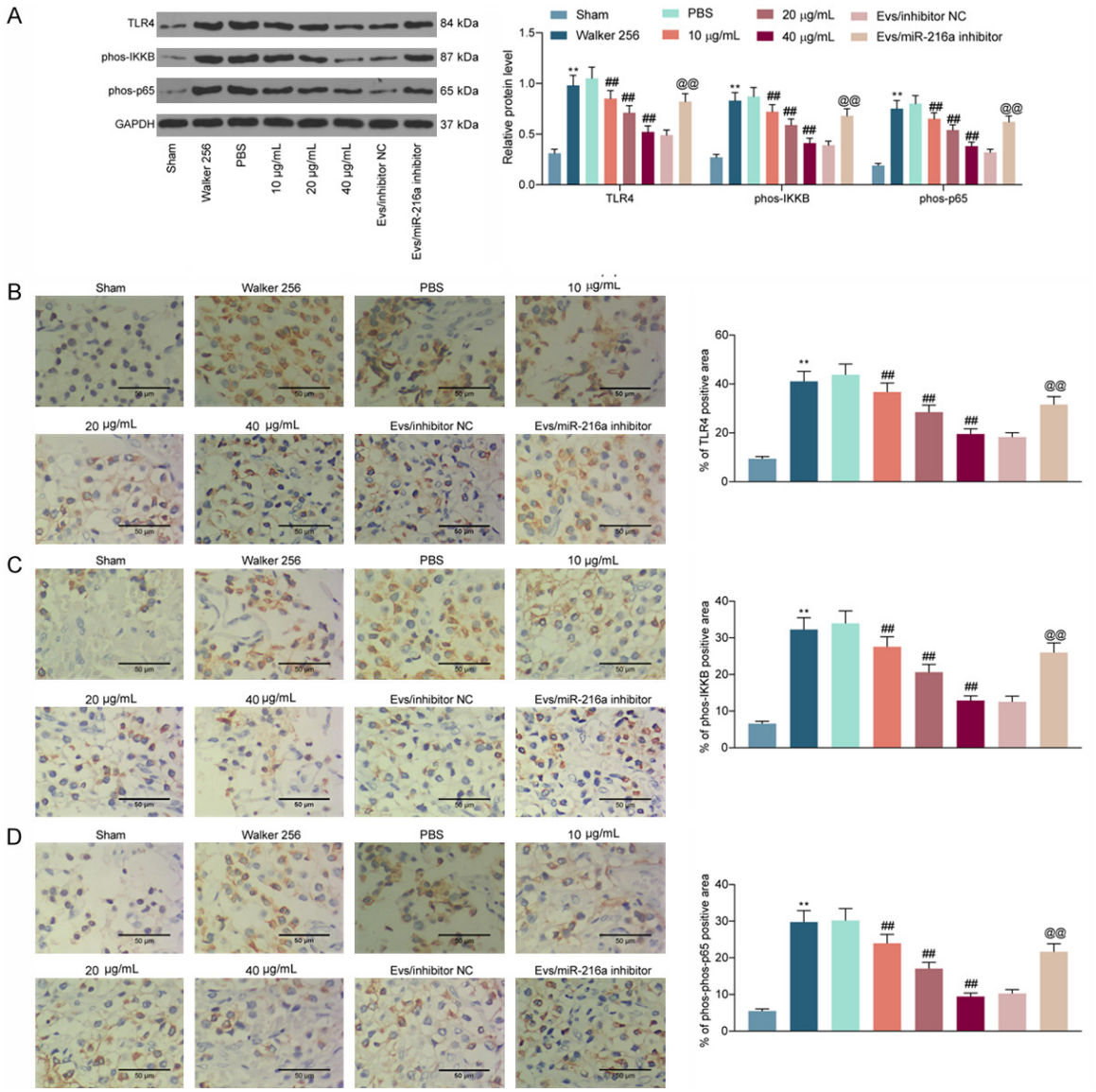

Figure 7. HMGB1 promotes nociception in CIBP mice by activating the TLR4-NF-κB signaling pathway. (A) Western blot detection of expression of TLR4 and the extent of IKKB and NF-κB p65 phosphorylation in the spinal cord of mice; (B-D) Immunohistochemical staining intensity of TLR4 (B), phos-IKKB (C), and phos-NF-κB p65 (D) in spinal cord tissues. n = 8. $^{**}P < 0.01$, $^{\#\#}P < 0.01$, $^{@@}P < 0.01$ as determined by one-way ANOVA (B-D) or two-way ANOVA (A), followed by Tukey's post-hoc analysis.

ry factors, including TNF-α, IL-1β and IL-6 in serum of CIBP mice. The anti-inflammatory role of M2φ-Evs has been highlighted in different disorders, including ulcerative colitis [17] and experimental autoimmune encephalomyelitisa [18]. Mechanistically, Moghaddam *et al.* proposed that M2φ secrete great amounts of IL-10 and TGF-β to curb the inflammation, resulting in tissue repair, remodeling, vasculogenesis and retain homeostasis [19]. Moreover, macrophages have remarkable functions in modulating neuroinflammation, thus being considered as a peripheral regulator of neuropathic pain [20]. Vakili *et al.* evidenced that M2φ-Evs possess neurotoxic effects in the context of neuroinflammation [21]. Nevertheless, the importance of M2φ-Evs in nociception of CIBP, to the best of our knowledge, has rarely been studied. Our findings established that M2φ-Evs exerted an antinociceptive effect in CIBP mice.

To probe the finer mechanism, we sorted to miRNA microarray to screen differentially expressed miRNAs in spinal cord tissues of PBS-treated and M2φ-Evs-treated mice. The following RT-qPCR corroborated that M2φ-Evs elicit-

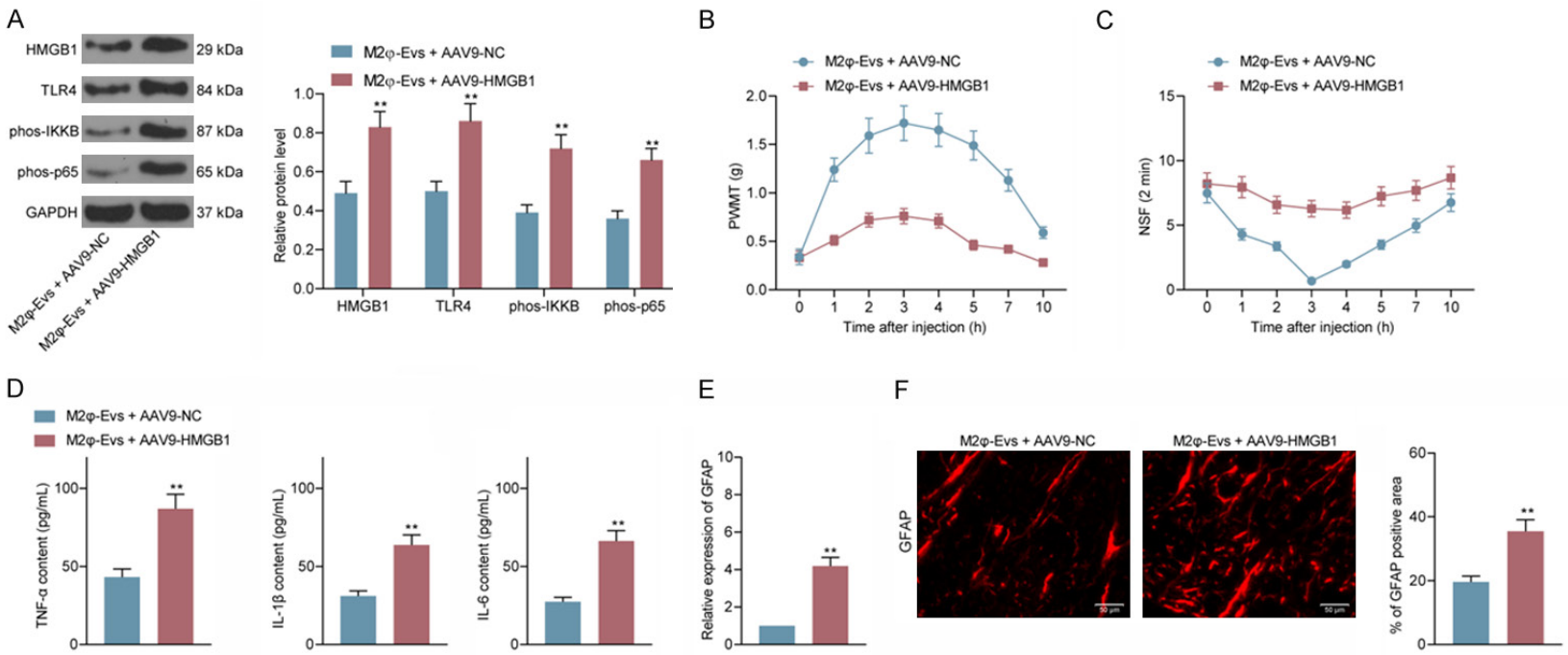

Figure 8. AAV9-HMGB1 attenuates the blocking effect of M2φ-Evs on the TLR4-NF-κB signaling pathway. Adenovirus overexpression vector harboring HMGB1 (AAV9-HMGB1) or empty vector (AAV9-NC) was injected into M2φ-Evs-treated mice via intrathecal injection. (A) The expression of HMGB1 and TLR4 and the phosphorylation levels of IKKB as well as NF-κB p65 in spinal cord tissues examined by western blot; (B) Mean (± SD) PWMT (in g) in response to five von Frey hair stimulations; (C) NSF in a time span of 2 min; (D) ELISA detection of inflammatory factors TNF-α, IL-1β, IL-6 in mouse serum; (E, F) Expression of the glial activation marker GFAP in mouse spinal cord tissues was detected by RT-qPCR (E) and immunofluorescence (F). n = 8. $^{**}P < 0.01$ as determined by unpaired *t* test (D-F) or two-way ANOVA (A-C), followed by Tukey's post-hoc analysis.

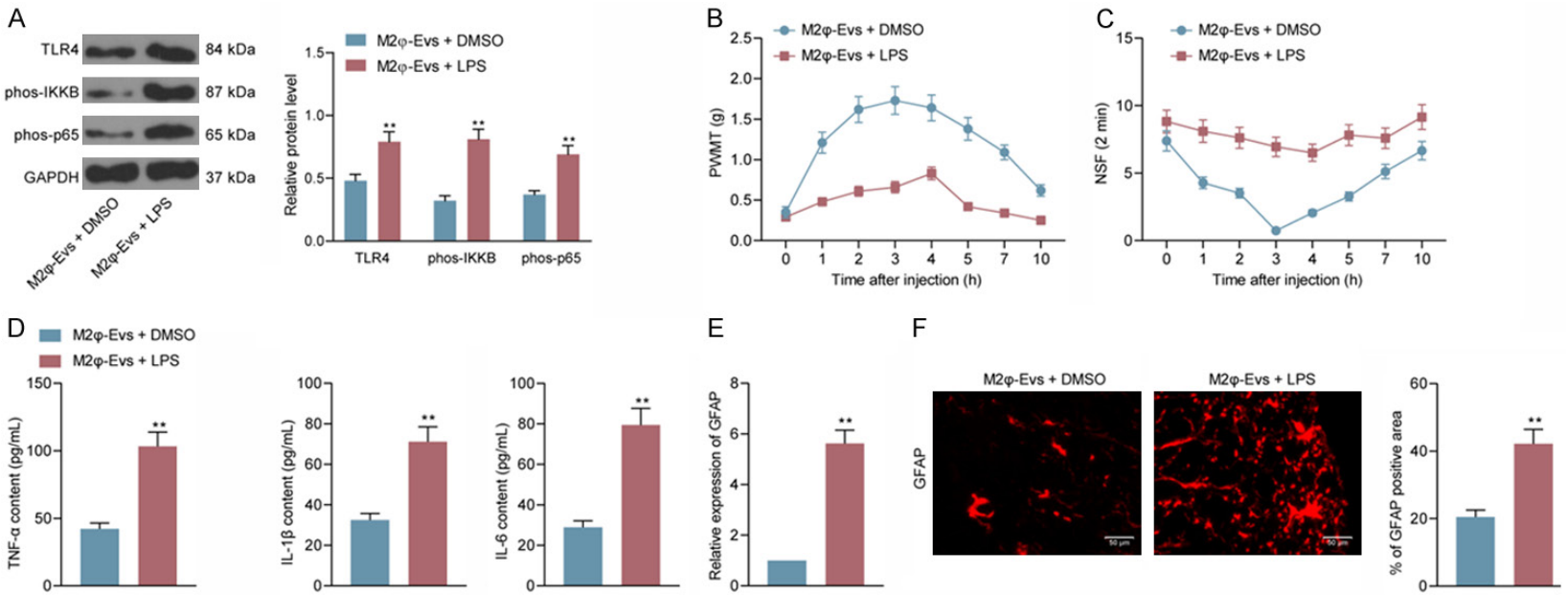

Figure 9. LPS attenuates the antinociceptive effect of M2φ-Evs on CIBP mice. LPS or DMSO was injected into M2φ-Evs-treated mice via intrathecal injection. (A) The expression of TLR4 and the phosphorylation levels of IKKB as well as NF-κB p65 in spinal cord tissues examined by western blot; (B) Mean (± SD) PWMT (in g) in response to five von Frey hair stimulations; (C) NSF in a time span of 2 min; (D) ELISA detection of inflammatory factors TNF-α, IL-1β, IL-6 in mouse serum; (E, F) Expression of the glial activation marker GFAP in mouse spinal cord tissues was detected by RT-qPCR (E) and immunofluorescence (F). n = 8. $^{**}P < 0.01$ as determined by unpaired *t* test (D-F) or two-way ANOVA (A-C), followed by Tukey's post-hoc analysis.

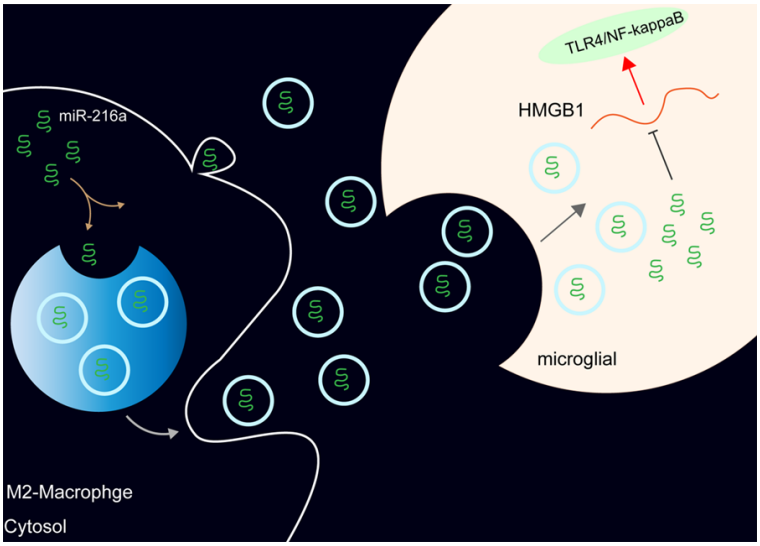

Figure 10. miR-216a carried by M2φ-Evs targets and negatively regulates HMGB1 expression, thereby blocking the TLR4-NF-κB signaling pathway.

ed antinociceptive effects on CIBP with the involvement of miR-216a. In line with our analysis, Saravanan detected exo-miR-216a-5p in islets, making it a possible diagnostic candidate for prediabetic conditions [22]. More specifically, endothelial cells co-cultured with miR-216a-5p-containing exosomes attenuated inflammatory response, as manifested by lowered IL-1β, IL-6, and TNF-α levels [23]. *In vivo*, exosome-shuttled miR-216a-5p from mesenchymal stem cells repaired spinal cord injury by changing M1/M2 polarization of microglials [24]. All these findings concur well with our results, which displayed that miR-216a inhibitor in M2φ led to higher IL-1β, IL-6, TNF-α levels in serum and GFAP activation in spinal cord tissues, while lower PWMT in CIBP mice.

With an aim to find out the downstream effector of miR-216a in CIBP, three bioinformatics websites were used. The filtered 155 genes were subjected to KEGG enrichment analysis, which revealed that the TLR4-NF-κB signaling was significantly enriched. Moreover, miR-300 has been found to mitigate CIBP through targeting HMGB1 in a rat model [25]. Also, the miR-216a/HMGB1/NF-κB axis has been reported in H_2O_2-induced 16HBE cell injury [26]. Therefore, we determined the HMGB1/TLR4-NF-κB regulatory axis as the downstream biomolecules of miR-216a in CIBP. HMGB-1, residing in eukaryotic nuclei and comprising 215 amino acid residues, interacts with RAGE and members of the TLR family, including TLR-4 to activate NF-κB which influences the release of proinflammatory cytokines [27]. Our western blot and immunohistochemistry results validated the overactivation of HMGB1 expression and TLR4-NF-κB pathway activity in CIBP mice. Further M2φ-Evs application blunted the pathway, while miR-216a inhibitor induced their expression and activity again. Similarly, miR-216a has the potency to inhibit the production of pro-inflammatory cytokine mediated by NF-κB in teleost fish by mediating p65 [28]. In addition, impairing the HMGB1-RAGE axis suppressed pro-inflammatory macrophages/microglia polarization and exerted neuroprotective effects following spinal cord injury in rats [29]. Moreover, celastrol could ameliorates the inflammatory pain via suppressing the activation of HMGB1/NF-κB signaling in dorsal root ganglion [30]. Furthermore, the simultaneous injection of lidocaine, a typical local anesthetic, and an HMGB1 antibody can further mitigate neuropathic pain and neuroinflammation in rats with spared nerve injury relative to the injection of lidocaine alone [31]. The rescue experiments conducted in the present work unveiled that overexpression of HMGB1 packaged by adenovirus vector and activation of the TLR4-NF-κB pathway using LPS abolished the relieving effect of M2φ-Evs on nociception in CIBP mice. Therefore, it is fair to conclude that the antinociceptive behaviors of miR-216a loaded by M2φ-Evs on CIBP mice were elicited through the HMGB1/TLR4-NF-κB axis deficit. Considering that our bioinformatics analyses show 155 genes are possible candidate for the target of miR-216a. Further studies are needed to test the possibility of other gene involvement.

Conclusion

The current investigation is the first to employ M2φ-Evs to examine the role of miR-216a on antinociceptive behaviors in CIBP mice. miR-216a loaded by M2φ-Evs attenuated Walker 256 cells-induced nociception in mice with CIBP by blocking the HMGB1/TLR4-NF-κB axis (**Figure 10**). These discoveries unquestionably

revealed a new chapter in the treatment of CIBP, which had potential application significance.

Acknowledgements

The authors would like to thank PhD research startup foundation of the First Affiliated Hospital of Kunming Medical University (2018-BS021). This work is supported by PhD research startup foundation of the First Affiliated Hospital of Kunming Medical University (2018-BS021).

Disclosure of conflict of interest

None.

Address correspondence to: Zhangxiang Huang, Department of Pain Management, The First Affiliated Hospital of Kunming Medical University, NO. 295, Xichang Road, Wuhua District, Kunming 650032, Yunnan, P. R. China. Tel: +86-15697055158; Fax: +86-15697055158; E-mail: Hzhangxiang9181@163.com; Zhiwen Yan, Department of Anatomy, Kunming Medical University Haiyuan College, NO. 389, Haiyuan North Road, Kunming 650101, Yunnan, P. R. China. Tel: +86-15697055158; Fax: +86-15697055158; E-mail: 149140108@qq.com

References

[1] Zhu XC, Zhang JL, Ge CT, Yu YY, Wang P, Yuan TF and Fu CY. Advances in cancer pain from bone metastasis. Drug Des Devel Ther 2015; 9: 4239-4245.

[2] Zajaczkowska R, Kocot-Kepska M, Leppert W and Wordliczek J. Bone pain in cancer patients: mechanisms and current treatment. Int J Mol Sci 2019; 20: 6047.

[3] Ellingson HM and Vanderah TW. Potential therapeutic treatments of cancer-induced bone pain. Curr Opin Support Palliat Care 2020; 14: 107-111.

[4] Mantyh P. Bone cancer pain: causes, consequences, and therapeutic opportunities. Pain 2013; 154 Suppl 1: S54-62.

[5] Park SH, Eber MR, Widner DB and Shiozawa Y. Role of the bone microenvironment in the development of painful complications of skeletal metastases. Cancers (Basel) 2018; 10: 141.

[6] Murray PJ. Macrophage Polarization. Annu Rev Physiol 2017; 79: 541-566.

[7] EL Andaloussi S, Mäger I, Breakefield XO and Wood MJ. Extracellular vesicles: biology and emerging therapeutic opportunities. Nat Rev Drug Discov 2013; 12: 347-357.

[8] Raposo G and Stoorvogel W. Extracellular vesicles: exosomes, microvesicles, and friends. J Cell Biol 2013; 200: 373-383.

[9] Buzas EI, Gyorgy B, Nagy G, Falus A and Gay S. Emerging role of extracellular vesicles in inflammatory diseases. Nat Rev Rheumatol 2014; 10: 356-364.

[10] McDonald MK, Tian Y, Qureshi RA, Gormley M, Ertel A, Gao R, Aradillas Lopez E, Alexander GM, Sacan A, Fortina P and Ajit SK. Functional significance of macrophage-derived exosomes in inflammation and pain. Pain 2014; 155: 1527-1539.

[11] Shenoy PA, Kuo A, Vetter I and Smith MT. The walker 256 breast cancer cell- induced bone pain model in rats. Front Pharmacol 2016; 7: 286.

[12] Philipp D, Suhr L, Wahlers T, Choi YH and Paunel-Gorgulu A. Preconditioning of bone marrow-derived mesenchymal stem cells highly strengthens their potential to promote IL-6-dependent M2b polarization. Stem Cell Res Ther 2018; 9: 286.

[13] Peters CM, Ghilardi JR, Keyser CP, Kubota K, Lindsay TH, Luger NM, Mach DB, Schwei MJ, Sevcik MA and Mantyh PW. Tumor-induced injury of primary afferent sensory nerve fibers in bone cancer pain. Exp Neurol 2005; 193: 85-100.

[14] Chaplan SR, Bach FW, Pogrel JW, Chung JM and Yaksh TL. Quantitative assessment of tactile allodynia in the rat paw. J Neurosci Methods 1994; 53: 55-63.

[15] Zhou J, Shuang O, Li J, Cai Z, Wu C and Wang W. miR-34a alleviates spinal cord injury via TLR4 signaling by inhibiting HMGB-1. Exp Ther Med 2019; 17: 1912-1918.

[16] Rossi M, Battafarano G, D'Agostini M and Del Fattore A. The role of extracellular vesicles in bone metastasis. Int J Mol Sci 2018; 19: 1136.

[17] Deng F, Yan J, Lu J, Luo M, Xia P, Liu S, Wang X, Zhi F and Liu D. M2 macrophage-derived exosomal-miR-590-3p attenuates DSS-induced mucosal damage and promotes epithelial repair via the LATS1/YAP/beta-catenin signalling axis. J Crohns Colitis 2021; 15: 665-677.

[18] Wu L, Xia J, Li D, Kang Y, Fang W and Huang P. Mechanisms of M2 macrophage-derived exosomal long non-coding RNA PVT1 in regulating Th17 cell response in experimental autoimmune encephalomyelitisa. Front Immunol 2020; 11: 1934.

[19] Shapouri-Moghaddam A, Mohammadian S, Vazini H, Taghadosi M, Esmaeili SA, Mardani F, Seifi B, Mohammadi A, Afshari JT and Sahebkar A. Macrophage plasticity, polarization, and function in health and disease. J Cell Physiol 2018; 233: 6425-6440.

[20] Kiguchi N, Kobayashi D, Saika F, Matsuzaki S and Kishioka S. Pharmacological regulation of neuropathic pain driven by inflammatory macrophages. Int J Mol Sci 2017; 18: 2296.
[21] Vakili S, Ahooyi TM, Yarandi SS, Donadoni M, Rappaport J and Sariyer IK. Molecular and cellular impact of inflammatory extracellular vesicles (EVs) derived from M1 and M2 macrophages on neural action potentials. Brain Sci 2020; 10: 424.
[22] Saravanan PB, Vasu S, Yoshimatsu G, Darden CM, Wang X, Gu J, Lawrence MC and Nazirudin B. Differential expression and release of exosomal miRNAs by human islets under inflammatory and hypoxic stress. Diabetologia 2019; 62: 1901-1914.
[23] Peng RR, Shang SX, Zhao LS and Long FQ. MiR-216a-5p-containing exosomes suppress rTp17-induced inflammatory response by targeting TLR4. Biosci Rep 2019; 39: BSR2019-0686.
[24] Liu W, Rong Y, Wang J, Zhou Z, Ge X, Ji C, Jiang D, Gong F, Li L, Chen J, Zhao S, Kong F, Gu C, Fan J and Cai W. Exosome-shuttled miR-216a-5p from hypoxic preconditioned mesenchymal stem cells repair traumatic spinal cord injury by shifting microglial M1/M2 polarization. J Neuroinflammation 2020; 17: 47.
[25] Liu C, Yang J, Liu H, Xia T and Zhang F. miR-300 mitigates cancer-induced bone pain through targeting HMGB1 in rat models. Genes Genomics 2020; 42: 309-316.
[26] Chaoyang Y, Qingfeng B and Jinxing F. MiR-216a-5p protects 16HBE cells from H2O2-induced oxidative stress through targeting HMGB1/NF-kB pathway. Biochem Biophys Res Commun 2019; 508: 416-420.
[27] Bohm MR, Schallenberg M, Brockhaus K, Melkonyan H and Thanos S. The pro-inflammatory role of high-mobility group box 1 protein (HMGB-1) in photoreceptors and retinal explants exposed to elevated pressure. Lab Invest 2016; 96: 409-427.
[28] Xu T, Chu Q, Cui J and Huo R. MicroRNA-216a inhibits NF-kappaB-mediated inflammatory cytokine production in teleost fish by modulating p65. Infect Immun 2018; 86: e00256-18.
[29] Fan H, Tang HB, Chen Z, Wang HQ, Zhang L, Jiang Y, Li T, Yang CF, Wang XY, Li X, Wu SX and Zhang GL. Inhibiting HMGB1-RAGE axis prevents pro-inflammatory macrophages/microglia polarization and affords neuroprotection after spinal cord injury. J Neuroinflammation 2020; 17: 295.
[30] Zhang X, Zhao W, Liu X, Huang Z, Shan R and Huang C. Celastrol ameliorates inflammatory pain and modulates HMGB1/NF-kappaB signaling pathway in dorsal root ganglion. Neurosci Lett 2019; 692: 83-89.
[31] Li M, Jiang H, Gu K, Sun X, Gu J, Li C and Wang G. Lidocaine Alleviates Neuropathic Pain and Neuroinflammation by Inhibiting HMGB1 Expression to Mediate MIP-1alpha/CCR1 Pathway. J Neuroimmune Pharmacol 2020; [Epub ahead of print].